Supporting Information

Chaotropic agents boosting the performance of photo-ionic cells

*Romain Bourdon[a], Pekka Peljo[a], Manuel A. Méndez[a], Astrid J. Olaya[a], Jelissa De Jonghe[b], Heron Vrubel[a] and Hubert H. Girault[a,]**

[a]Laboratoire d'Electrochimie Physique et Analytique, Ecole Polytechnique Fédérale de Lausanne, CH-1015 Lausanne, Switzerland

[b]Groupe de Dynamique Photochimique, Ecole Polytechnique Fédérale de Lausanne, CH-1015 Lausanne, Switzerland

Contents

1 Electrochemistry

1.1 Cyclic Voltammetry

The CV of Azure B is shown in Figure S1A and the dependency of the peak current on the square root of the scan rate is shown in Figure S1B. The diffusion coefficient of 4.4 x 10^{-6} cm^2 s^{-1} was calculated from Randles–Ševčík equation with n = 2. Fig. S1B shows that the fit does not run through the origin. This is probably due to the redox reaction itself: the reaction is not simple two-electron reaction, but can be actually described as ET followed by fast disproportionation. The differences between these two cases are more readily observed at higher scan rates. Leaving out the two fastest scan rates would decrease the observed diffusion coefficient by *ca*. 10 %, with the fit running closer to the origin.

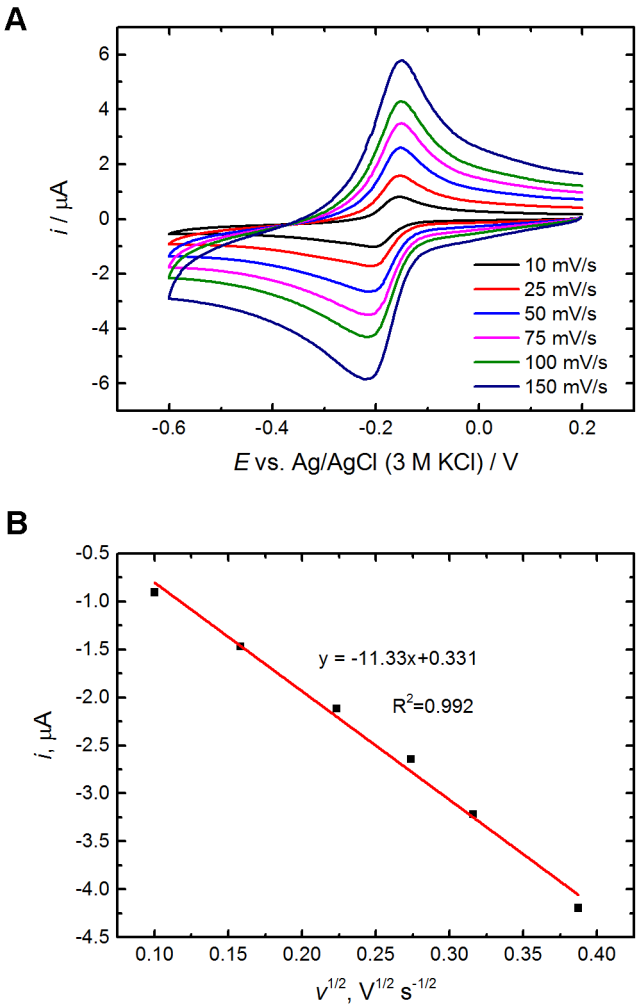

Figure S1. A) The scan rate dependency of the reduction of 0.1 mM Azure B in pH 7.2 phosphate buffer in deoxygenated solution at 3 mm diameter GC electrode.

CVs of Azure B in the presence of 8 M urea at different pH used for the construction of the Pourbaix diagram are shown in Figure S2

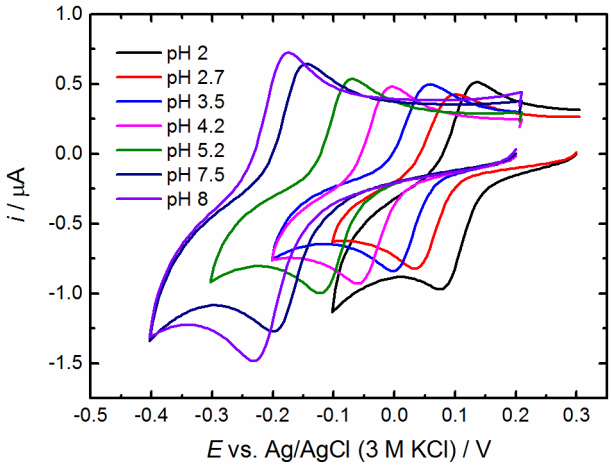

Figure S2. CVs of Azure B at different pH used for construction of the Pourbaix diagram.

1.2 Ion Transfer Voltammetry

The ion transfer voltammetry of 0.1 mM Azure B in pH 7.2 phophate buffer is shown in Figure S3. The Galvani potential scale was calibrated by addition of tetramethylammonium (TMA^+) into the cell. The Galvani potential difference across the interface ($\Delta_o^w\phi$) was estimated by taking the standard ion transfer potential of tetramethylammonium cation (TMA^+) as 0.160 V.[1]

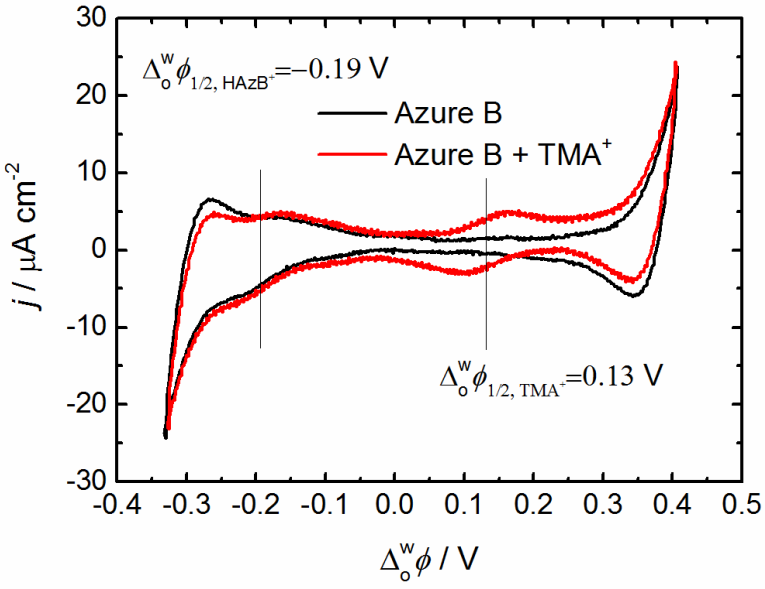

Figure S3. Ion transfer voltammetry of 0.1 mM Azure B in pH 7.2 phosphate buffer.

The half-wave potential of TMA^+ was estimated as 0.13 V based on correction of ionic activities by Debye-Hückel theory as described by Wandlowski *et al.*[1] Hence the half-wave potential of $HAzB^+$ was estimated as –0.195 V, and the calculated standard

transfer potential $\Delta_{\mathrm{o}}^{\mathrm{w}}\phi^{0}_{\mathrm{HAzB^+}} = -0.166$ V and the standard transfer energy $\Delta_{\mathrm{o}}^{\mathrm{w}}G^{0}_{\mathrm{HAzB^+}} = -16$ kJ mol^{-1}.

2 Transient Absorption Spectroscopy

Figure S4 shows the transient absorption spectra of the triplet state.

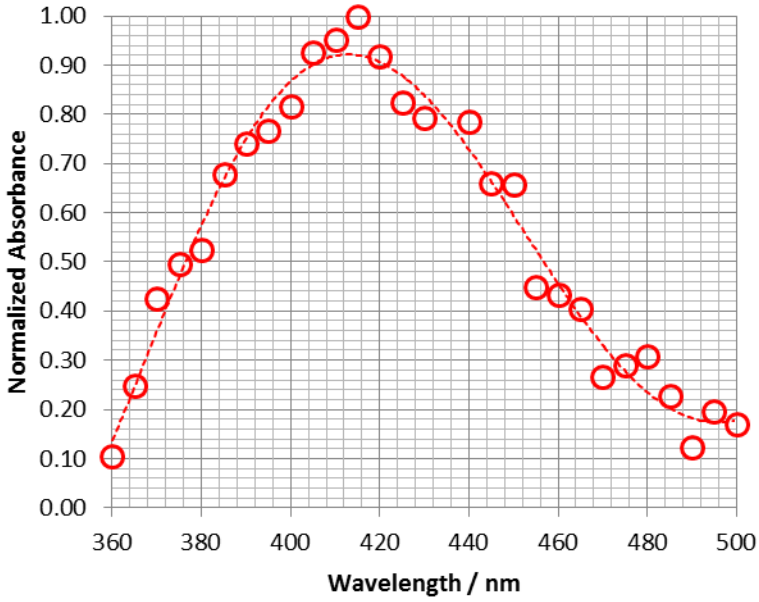

Figure S4. Absorption spectra of the triplet state recorded with transient absorption (5 μm $HAzB^+$).

3 Absorbance of Monomers and Dimers

The dimerization between dye D^+ takes place according to the following reaction

$$2\ D^+ \rightleftharpoons D_2^{2+} \qquad \text{(S1)}$$

The equilibrium constant K_D for the dimerization is given as follows, and the mass balance equation must hold.

$$K_D = \frac{\left[D_2^{2+}\right]}{\left[D^+\right]^2} \qquad \text{(S2)}$$

$$c_{\mathrm{tot}} = \left[D^+\right] + 2\left[D_2^{2+}\right] = \left[D^+\right] + 2K_D\left[D^+\right]^2 \qquad \text{(S3)}$$

Now concentrations of monomers and dimers can be solved from these equations:

$$\left[\mathrm{D}^{+}\right]=\frac{-1+\sqrt{1+8K_D c_{\mathrm{tot}}}}{4K_D} \tag{S4}$$

$$\left[\mathrm{D}_2^{2+}\right]=\frac{c_{\mathrm{tot}}-\left[\mathrm{D}^{+}\right]}{2} \tag{S5}$$

Absorbance can now be calculated with Lambert-Beer law:

$$A=\varepsilon_{\mathrm{M}} b\left[\mathrm{D}^{+}\right]+\varepsilon_{\mathrm{D}} b\left[\mathrm{D}_2^{2+}\right]=\varepsilon_{\mathrm{M}} b\frac{\sqrt{1+8K_D[\mathrm{D}^{+}]}-1}{4K_D}+\varepsilon_{\mathrm{D}} b\left(\frac{c_{\mathrm{tot}}}{2}-\frac{\sqrt{1+8K_D[\mathrm{D}^{+}]}-1}{8K_D}\right) \tag{S6}$$

where K_D represents the dimerization constant. ε_{M} and ε_{D} stand for the molar extinction coefficients of the monomeric and dimeric species, respectively, b is the path length. The parameters in equation S6 can be fitted with experimental absorbance data to estimate the dimerization constant, and the ratios of dimers and monomers with and without urea for Azure B as a function of concentration is given in Figure S5.

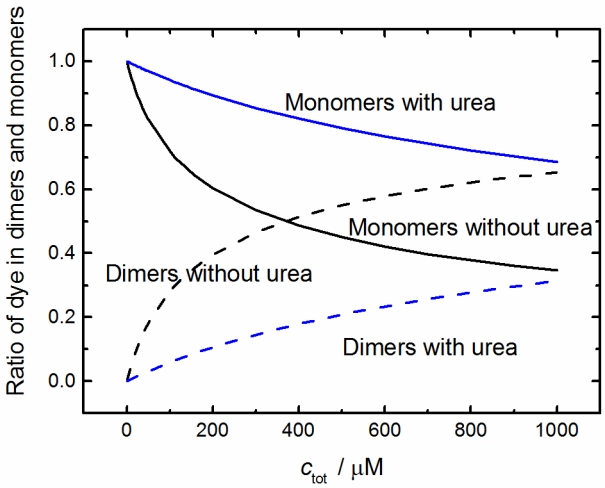

Figure S5. The ratio of dye in monomers and dimers. Dashed lines for dimers and solid lines for monomers (black lines: [Urea] = 0 M, blue lines [Urea] = 8 M).

3 Model for the Light Absorption, Photoreaction and Extraction

As the real mechanism of the photoreactions would be too complicated for the simulations (see Scheme 1 in the main text), the approach described in the previous publication was chosen to be utilized for estimation of the performance of the droplet systems. In the system the photoexcited dye A will form the photoexcited state A*, with the average lifetime of the photoexcited state of τ. The governing reactions are

photoexcitation of A, followed by reaction with electron donor R producing B and O, or relaxation of the excited state A* back to A.

$$\mathrm{A} \xrightarrow{h\nu} \mathrm{A}^* \tag{S7}$$

$$\mathrm{A}^* + \mathrm{R} \xrightarrow{k_{photo}} \mathrm{B} + \mathrm{O} \tag{S8}$$

The reduced dye can be oxidized by O in the recombination reaction:

$$\mathrm{B} + \mathrm{O} \xrightarrow{k_{rec}} \mathrm{A} + \mathrm{R} \tag{S9}$$

or B can be extracted into the oil phase.

The absorption of light is described by Eq. S10.

$$\P I / \P x = - \epsilon c_{\mathrm{A}} I \tag{S10}$$

where I is the light intensity, ε the extinction coefficient of A and c_{A} is the concentration of A. The light at the intensity of I_0 is shining through the light electrode at $x = 0$. In the steady state the transport and kinetics of A is:

$$\nabla \cdot \left(D_{\mathrm{A}} \nabla c_{\mathrm{A}} \right) - \mathbf{u} \cdot \nabla c_{\mathrm{A}} - \phi \varepsilon c_{\mathrm{A}} I + k_{rec} c_B c_O + \frac{c_{\mathrm{A}*}}{\tau} = 0 \tag{S11}$$

where ϕ is the quantum efficiency for the generation of B, k_{rec} is the recombination rate constant and τ is the lifetime of the excited state. **u** is the velocity field. To have the correct units for all the terms in Eq. (S11), the light intensity has to be expressed as molar flux of photons (mol cm^{-2} s^{-1}), as described earlier by Albery *et al.*[2] Correspondingly for other species

$$\nabla \cdot \left(D_{\mathrm{A}*} \nabla c_{\mathrm{A}*} \right) - \mathbf{u} \cdot \nabla c_{\mathrm{A}*} + \phi \varepsilon c_{\mathrm{A}} I - k_{photo} c_{\mathrm{A}*} c_R - \frac{c_{\mathrm{A}*}}{\tau} = 0 \tag{S12}$$

$$\nabla \cdot \left(D_{\mathrm{R}} \nabla c_{\mathrm{R}} \right) - \mathbf{u} \cdot \nabla c_{\mathrm{R}} - k_{photo} c_{\mathrm{A}*} c_R + k_{rec} c_B c_O = 0 \tag{S13}$$

$$\nabla \cdot \left(D_B \nabla c_{\mathrm{B}} \right) - \mathbf{u} \cdot \nabla c_{\mathrm{B}} + k_{photo} c_{\mathrm{A}*} c_R - k_{rec} c_B c_O = 0 \tag{S14}$$

$$\nabla \cdot \left(D_{\mathrm{O}} \nabla c_{\mathrm{O}} \right) - \mathbf{u} \cdot \nabla c_{\mathrm{O}} + k_{photo} c_{\mathrm{A}*} c_R - k_{rec} c_B c_O = 0 \tag{S15}$$

The reduced dye B can partition into the oil phase, with the partition coefficient defined as:

$$K = \frac{c_{\mathrm{B}}^{\mathrm{oil}}}{c_{\mathrm{B}}^{\mathrm{aq}}} = \frac{k_f}{k_b} \tag{S16}$$

Where k_f and k_b are rate constants for the transfer of B from aqueous phase to DCE phase. This was implemented into the flux boundary condition as described below:

$$D_{\mathrm{B,DCE}}\left(\frac{\partial c_{\mathrm{B,DCE}}}{\partial x}\right)_{x=0} = -D_{\mathrm{B,aq}}\left(\frac{\partial c_{\mathrm{B,aq}}}{\partial x}\right)_{x=0} = k_f c_{\mathrm{B,aq}} - k_b c_{\mathrm{B,DCE}} \tag{S17}$$

This set of equations was used to estimate the phase separation in the steady state conditions in 1D. Experimental results were used to tune the parameters, and axial symmetry 2D simulations of droplets in a flow were performed to evaluate the effects of the droplet radius on the system performance. The simulated system consisted of a stationary droplet of water in a flow of DCE phase. The convection in both phases was described by two Navier-Stokes equations for the incompressible Newtonian fluids, one in each phase:

$$\rho(\mathbf{u}\cdot\nabla\mathbf{u}) = -\nabla p + \mu\nabla^2\mathbf{u} \tag{S18}$$

Where ρ is the density of the material, p is pressure, and μ is dynamic viscosity of the fluid. The inlet boundary condition for the DCE phase was set as terminal velocity of the droplet, and the outlet at the bottom was set at 1 atm pressure. The tangential velocity at the liquid-liquid interface was set same on both phases, and no-slip condition was used for the outer boundary of the system The values of water at room temperature were used for both density and viscosity of the aqueous phase, and correspondingly the density and viscocity of DCE at 20 °C were used for DCE phase.

For all the species, the boundary conditions at the inflows was constant concentration, and outflow at the outlets (c = 0). The cell walls were set as insulating (no flux through the boundary), and axial symmetry was applied at the boundary r = 0. The initial values were $c_{\mathrm{A}} = c_{\mathrm{A,0}}$, $c_{\mathrm{B}} = 0$, $c_{\mathrm{O}} = 0$ and $c_{\mathrm{R}} = c_{\mathrm{R,0}}$. The light was transmitted through the bottom of the cell at the intensity of I_0.

3.1 Model Parameters

As thionine and Azure B have very similar photophysical behavior and redox potential, the kinetic parameters used in the previous model were modified so that the 1D model reproduced the experimental steady-state extraction of 83.3 %. The lifetime of Azure B of 18 μs and partition coefficient of 6.1 determined in this work were used, and the model parameters are shown in Table S1.

Table S1. Model parameters

Name	Expression	Description
ε	2×10^4 M^{-1} cm^{-1}	Extinction coefficient of the dye[a]
I_0	6.4×10^{-3} mol m^{-2} s^{-1}	Light intensity converted to molar flux (1234 W m^{-2} at 625 nm)
S^+_0	0.5 mM	Initial dye concentration in the aqueous phase
S_0	0 mM	Initial reduced dye concentration in the aqueous phase
R_0	600 mM	Concentration of reduced quencher species
O_0	0 mM	Concentration of oxidized quencher species
τ	18×10^{-6} s	Lifetime of the excited state of the dye[a]
K	6.1	Experimental partition coefficient of the dye (*vide infra*)
k_f	$k_b \times K$	Rate of transfer to oil
k_b	1 m s^{-1}	Rate of transfer to water
k_{rec}	3.5×10^4 M^{-1} s^{-1}	Recombination rate estimated from 1D simulations
k_q	1×10^7 M^{-1} s^{-1}	Quenching rate estimated from 1D simulations
D_{CoEDTA}	5.35×10^{-6} cm^2 s^{-1}	Diffusion coefficient of [Co(II)EDTA]$^{2-}$ at pH 7[3]
$D_{\mathrm{HAzB+}}$	2.2×10^{-6} cm^2 s^{-1}	Diffusion coefficient of Azure B[a]

[a]This work

Terminal velocities of spherical droplets were estimated according to Wallis.[4] Firstly, dimensionless radius and velocity are defined as

$$a^* = a\left(\frac{\rho_f g\Delta\rho}{\mu_c^{\,2}}\right)^{1/3} \tag{S19}$$

$$v^* = v\left(\frac{\rho_f^{\,2}}{\mu_c g\Delta\rho}\right)^{1/3} \tag{S20}$$

where subscript c refers to the continuous phase, ρ is density, μ is dynamic viscosity, a is radius of the droplet, v is terminal velocity, and g is standard acceleration due to gravity. For small droplets ($r^* < 1.5$) the dimensionless velocity is given by

$$v^* = \frac{2}{9}(a^*)^2\left(\frac{3\mu_d + 3\mu_c}{3\mu_d + 2\mu_c}\right) \tag{S21}$$

where subscript d refers to droplet phase. For larger droplets ($1.5 < r^* < 13.4$) the terminal velocity is given by $v^* = 0.408a^{*1.5}$ and for even larger droplets by

$$v^* = \frac{(a^*)^2}{9} \tag{S22}$$

At 293.15 K the density of water is 0.9982 g cm^{-3} and density of 1,2-dichloroethane is 1.257 g cm^{-3} and the corresponding viscosities are 1.005 mPa s and 0.844 mPa s. The terminal velocities calculated based on these equations are shown in Table S2.

3.2 Model Validation

The validation of the 1D model has been shown earlier.[5] The model was solved numerically by utilizing finite element based software COMSOL Multiphysics 4.4. The Navier-Stokes model was validated by comparison of the numerical solution for the 10 μm radius droplet with the analytical solution obtained by Hadamart-Rybczynski solution, given by stream functions in polar coordinates (r, θ) for inside and outside of the droplet (with the center of the droplet at (0,0)[6]:

$$\hat{\psi} = \frac{v r^2 \sin^2\theta}{4(1+\kappa)}\left[1-\frac{r^2}{a^2}\right] \tag{S23}$$

$$\psi = -\frac{v r^2 \sin^2\theta}{2}\left[1-\frac{a(2+3\kappa)}{2r(1+\kappa)}+\frac{\kappa a^3}{2r^3(1+\kappa)}\right] \tag{S24}$$

where $\kappa = \mu_c/\mu_d$. The velocities in radial and angular direction can be evaluated from

$$v_r = \frac{1}{r^2\sin\theta}\frac{\partial\psi}{\partial\theta} \text{ and } v_\theta = \frac{-1}{r\sin\theta}\frac{\partial\psi}{\partial r} \tag{S25}$$

The velocity vector can then be transformed into the Cartesian coordinates:

$$\mathbf{v} = v_r\cdot\mathbf{s} + v_\theta\cdot\boldsymbol{\varphi} = v_r\cdot(\cos\theta\mathbf{i}+\sin\theta\mathbf{j}) + v_\theta\cdot(-\sin\theta\mathbf{i}+\cos\theta\mathbf{j}) = (v_r\cos\theta - v_\theta\sin\theta)\mathbf{i} + (v_r\sin\theta + v_\theta\cos\theta)\mathbf{j} \tag{S26}$$

where **s** and **φ** are the unit vectors in radial and angular directions and **i** and **j** are the Cartesian unit vectors. The results can be changed to the Cartesian coordinates (x, y) by substituting $r = \sqrt{x^2+y^2}$ and $\theta = \arctan(y/x)$, resulting for the velocities inside the droplet as

$$v_x = \frac{v\left(a^2-x^2-2y^2\right)}{2a^2(1+\kappa)} \text{ and } v_y = \frac{vxy}{2a^2(1+\kappa)} \tag{S27}$$

and in the continuous phase as

$$v_x = -\frac{v\left(a^3\kappa\left(2x^2-y^2\right)+4(1+\kappa)\left(x^2+y^2\right)^{5/2}-a(2+3\kappa)\left(2x^4+3x^2y^2+y^4\right)\right)}{4(1+\kappa)\left(x^2+y^2\right)^{5/2}} \text{ and}$$

$$v_y = \frac{vaxy\left(-3a^3\kappa+(2+3\kappa)\left(x^2+y^2\right)\right)}{4(1+\kappa)\left(x^2+y^2\right)^{5/2}} \tag{S28}$$

Figure S6 shows the comparison of the analytical and numerical solutions for the velocity profile from the center of the droplet towards the wall, perpendicular to the flow direction, at different wall distances for a 10 μm radius droplet. Positive velocity indicates flow up, and negative velocity is flow down. Distance is normalized by the droplet radius and velocity by terminal velocity.

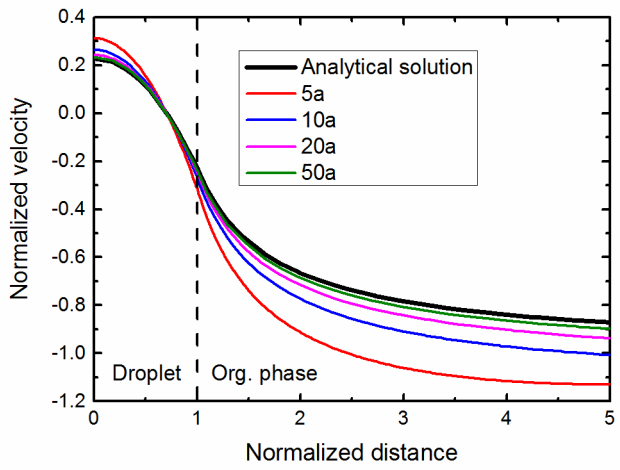

Figure S6. Velocity profiles from the center of the droplet towards the wall for different wall distances, *a* is the radius of the droplet.

As seen from the Figure S6, the velocity profile approaches the analytical solution for the flow in infinite medium when the wall distance increases. At the distance of 10 *a* the deviation from the analytical solution at the center of the droplet is 16 %, decreasing to 7 % for the wall distance of 20 *a*. However, if the same analysis is performed for the 1000 μm radius droplet, where the flow conditions deviate from the creeping flow behavior, the decrease of the wall distance from 25 *a* to 5 *a* results in the change of 3 % for the velocity observed at the centre of the droplet. Hence acceptable wall distance is 20 *a* for small droplets and 5 *a* for larger droplets (> 100 μm radius).

The full model was validated by increasing the mesh density for a 10 μm radius droplet, until the results did not significantly change. However, it was found out that the mesh density was more critical with the big droplet sizes (300-1000 μm radius). Unfortunately, further increment of the mesh density at the large droplets was not practical due to the time required to solve the model increasing to several days. Hence the accuracy of the numerical solution is better for the smaller droplets.

3.3 Model Results

The model was solved numerically by utilizing finite element method based software COMSOL Multiphysics 4.4. The model was solved sequentially by first solving the velocity profiles from the Navier-Stokes models in steady-state conditions, then solving the equations for light absorption in steady-state conditions. Then the transport equations for all the species were solved together with the light absorption as a function of time, taking the velocity profiles from the steady-state solution and using the steady-state light absorption as an initial condition. The normalized velocity profiles for all the simulated droplet sizes are shown in Figure S7, clearly showing the transition of the flow from creeping flow conditions (< 100

μm radius) to laminar flow conditions. The higher terminal velocity affects the velocity at the droplet boundary, leading to higher recirculation velocities.

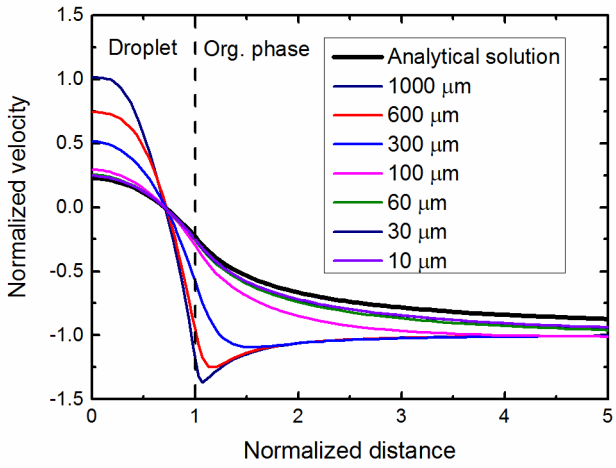

Figure S7. Normalized velocity profiles for all the simulated droplet sizes. Wall distance 50 *a*.

Examples of light intensity, velocity profile and concentration of the dye and photoproduct are shown in figures S8-S10.

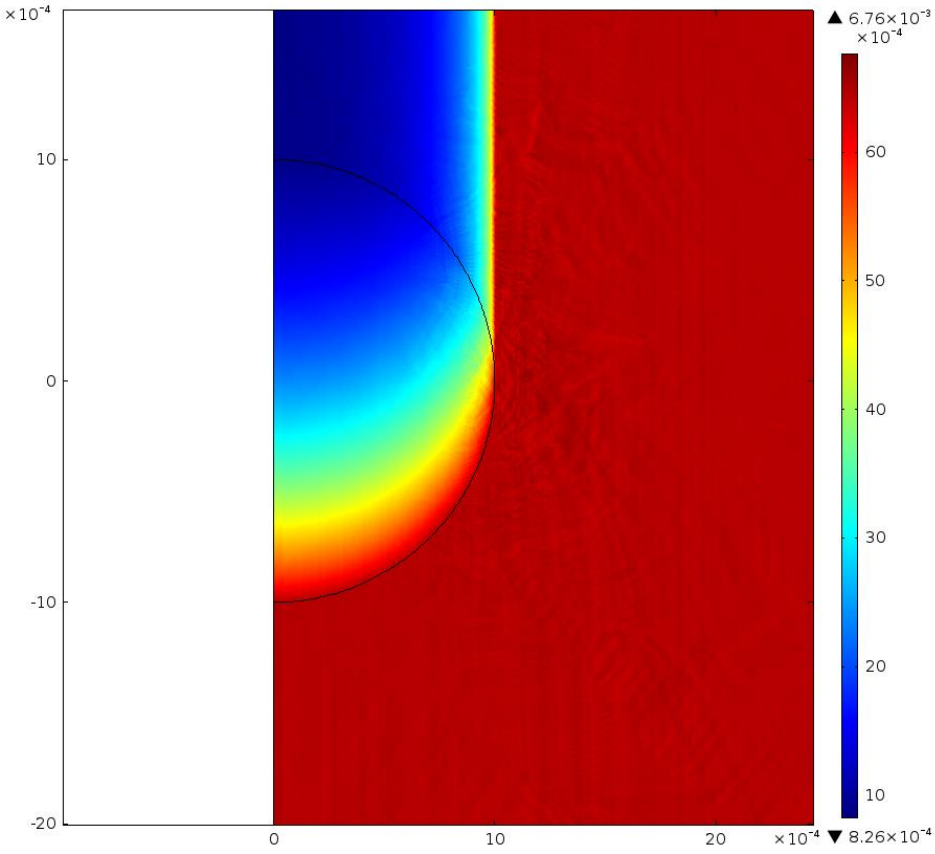

Figure S8. Simulated light intensity profile at t = 0 s, 1 mm radius droplet. The light input from below is 6.4×10^{-3} mol m^{-2} s^{-1}.

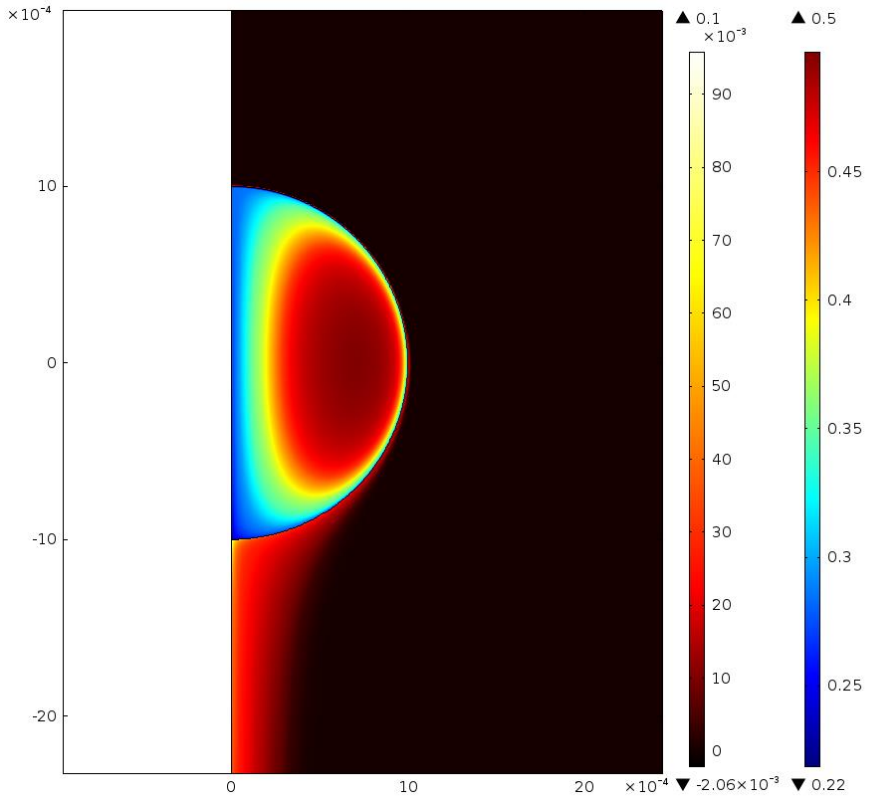

Figure S9. Simulated concentrations of dye inside the droplet and leucodye outside of the droplet at t = 0.3 s, 1 mm radius droplet moving up at terminal velocity. The initial dye concentration in the aqueous droplet was 0.5 mM.

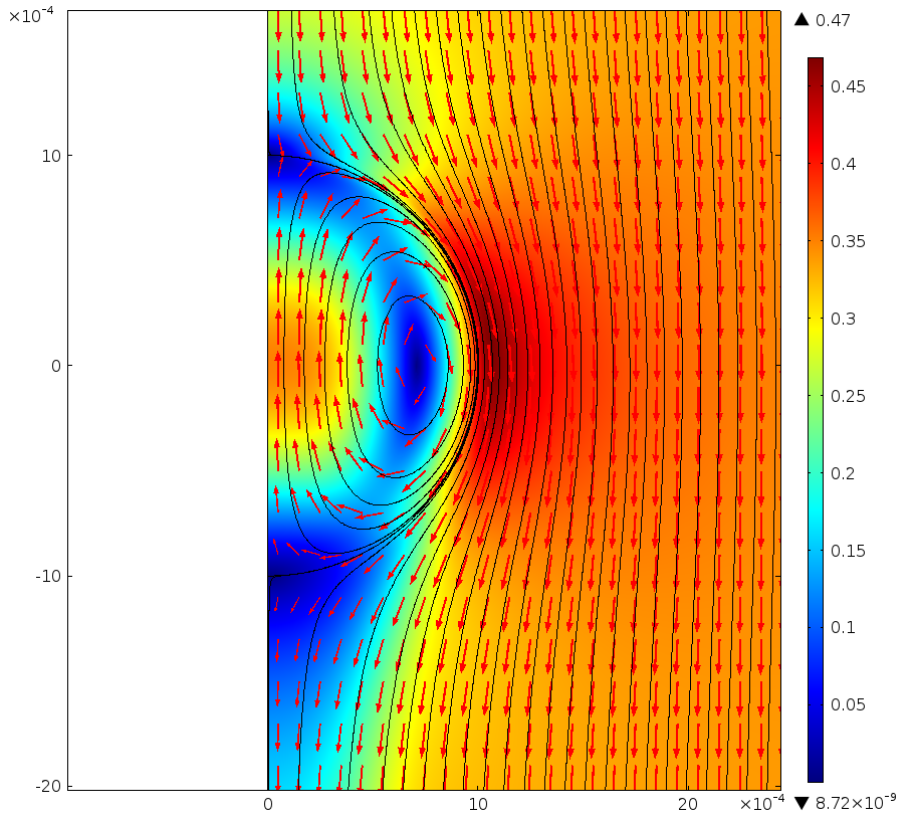

Figure S10. Simulated velocity profile for 1 mm radius droplet stationary in a downward flow at terminal velocity of 0.34 m/s.

Several parameters were evaluated from the models, like the time to consume half of the dye in the droplet ($t_{1/2}$), time of the conversion of half of the initial amount of dye into the photoproduct in the organic phase ($t_{product,1/2}$), and quantum yield (amount of photoproduct divided by the amount of adsorbed photons, η). Additionally, the distance travelled during the $t_{1/2}$ (x_1) and $t_{product,1/2}$ (x_2) were calculated from the terminal velocity (v), and these values are shown in Table S2.

Table S2. Different parameters evaluated from the numerical simulations.

r / μm	$t_{1/2}$ / s	$t_{product,1/2}$ / s	η, %	x_1, cm	x_2, cm	v, m/s
10	0.087	0.13	44.8	0.00069	0.0011	0.000079
30	0.19	0.42	17.3	0.013	0.030	0.00071
60	0.36	0.81	8.82	0.10	0.23	0.0029
100	0.53	1.4	5.07	0.51	1.3	0.0096
300	1.1	2.5	3.30	5.2	12	0.050
600	0.87	1.8	4.88	12	25	0.14
1000	0.71	1.2	7.85	23.7	39.9	0.34

As seen from Table S2, at first the time to bleach half of the dye increases until the droplet size of 100 μm, and the quantum yield decreases due to the increasing time for the recombination to take place. However, the bigger droplets show again decrease in $t_{1/2}$, and increase in the quantum yield, due to the improved tangential velocity observed at higher velocities when system moves from creeping flow behavior to laminar flow region. The uncertainty of the model at higher velocities is higher because the model does not account for the droplet deformation. As the terminal velocity of big droplets is significantly higher, the distances to perform half of the reaction increase substantially with increasing droplet size, from 0.001 cm to 40 cm.

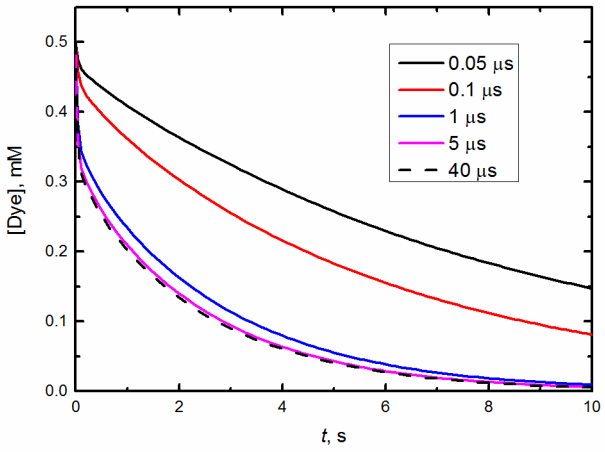

Figure S10. Dye concentration in the 100 μm radius droplet as a function of time for different excited state lifetimes.

Interestingly, excited state lifetime of the dye had small effect on the dye concentration for 100 μm radius droplet. Only the decrease of the lifetime below 1 μs had some effects on the photoreaction performance, as seen from Figure S10. This is

because the convection inside the droplet is high enough that the diffusion is not limiting the extraction.

4 References

(1) Wandlowski, T.; Mareček, V.; Samec, Z. *Electrochim. Acta* **1990**, *35*, 1173.

(2) Albery, W. J.; Archer, M. D. *Nature* **1977**, *270*, 399.

(3) Furukawa, K.; Takahashi, Y.; Sato, H. *Geochim. Cosmochim. Acta* **2007**, *71*, 4416.

(4) Wallis, G. B. *Int. J. Multiphase Flow* **1974**, *1*, 491.

(5) Méndez, M. A.; Peljo, P.; Scanlon, M. D.; Vrubel, H.; Girault, H. H. *J. Phys. Chem. C* **2014**, *118*, 16872.

(6) Clift, R.; Grace, J. R.; Weber, M. E. *Bubbles, Drops, and Particles*; Academic Press: New York, 1978.